

# Plasmonic Breathing and Edge Modes in Aluminum Nanotriangles

Alfredo Campos,<sup>†</sup> Arnaud Arbouet,<sup>‡</sup> Jérôme Martin,<sup>§</sup> Davy Gérard,<sup>§</sup> Julien Proust,<sup>§</sup> Jérôme Plain,<sup>§</sup> and Mathieu Kociak\*,<sup>†</sup>

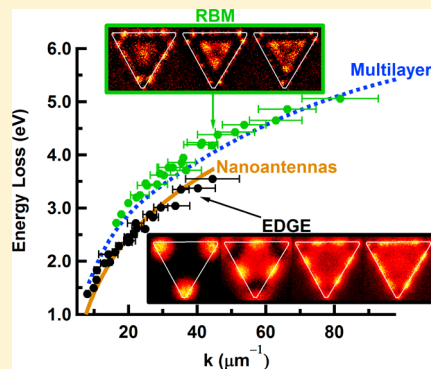
<sup>†</sup>Laboratoire de Physique des Solides, Bâtiment 510, UMR CNRS 8502, Université Paris Sud, Orsay 91400, France

<sup>‡</sup>CEMES, UPR 8011, CNRS-Université de Toulouse, 29 Rue Jeanne Marvig, BP 94347, F-31055 Toulouse, France

<sup>§</sup>Laboratoire de Nanotechnologie et Instrumentation Optique (LNIO), Institut Charles Delaunay, UMR CNRS 6281, Université de Technologie de Troyes, Troyes 10004, France

## S Supporting Information

**ABSTRACT:** We use electron energy loss spectroscopy (EELS) to perform a comprehensive spectroscopy and mapping of the plasmonic modes sustained by aluminum nanotriangles. Behind the apparent simplicity of such structures, a rich variety of plasmonic modes is observed. Edge modes and pseudoradial breathing modes (pseudo-RBMs) are unveiled as they couple efficiently with the electron source. We propose analytical models confirmed by rigorous simulations to index both families of modes and describe their spatial symmetry. Edge modes could be indexed as nanoantenna modes, while pseudo-RBMs match triangular cavities ones. The dispersion relation of both modes is measured highlighting their different nature. Plasmonic resonances ranging from near-infrared (IR) to ultraviolet (UV) are obtained by varying the triangle sizes, and especially, we found pseudo-RBMs resonances in the UV region, making them interesting for UV applications.



**KEYWORDS:** electron energy-loss spectroscopy, electron beam lithography, surface plasmon, edge mode, breathing mode, aluminum plasmonic

The optical properties of nanometric metallic particles have been studied for several decades, at first in the visible and infrared spectra<sup>1–3</sup> and more recently in the UV.<sup>4–6</sup> It is well-known that optical properties of metallic nanoparticles are dominated by surface plasmons that are collective electron oscillations at a metal-dielectric interface. In a metallic nanoparticle these oscillations are confined inside the boundaries of the particle, which can be tuned by shaping the geometry, resizing the nanoparticle or changing the dielectric environment. Recently, a detailed analysis of surface plasmons in flat structures<sup>7</sup> proposed to classify surface plasmon modes into two families. The first one corresponds to the so-called edge modes, which are localized at the periphery of two-dimensional nanoobjects. These edge modes are well-known in the literature and have been reported for several geometries.<sup>7–11</sup> On the other hand, the second group of modes corresponds to the so-called radial breathing modes (RBMs), which are localized inside the two-dimensional nanoobjects. Such modes have been reported experimentally for silver nanodisks,<sup>7,8</sup> silver nanosquares,<sup>10</sup> and silver nanotriangles.<sup>11–14</sup> Moreover, although a large number of studies have been performed on 2D plasmonic objects, only the plasmonics disks<sup>7,8</sup> received a comprehensive description. In contrast, the widely studied case of triangular prisms could not be comprehensively described, each study leading only to a partial understanding of the mode structure (Nelayah et al.,<sup>11,12</sup> Keast et al.,<sup>13</sup> Hao et al.,<sup>14</sup> Kumar et al.,<sup>15</sup> Fung et al.,<sup>16</sup> Pabitra et al.,<sup>17</sup> and Koh et al.).<sup>18</sup>

Here, we report on high-resolution imaging and spectroscopy of plasmon modes sustained by aluminum nanotriangles using electron energy loss spectroscopy (EELS) performed in a scanning transmission electron microscope (STEM). Through spectral and spatial mapping, we unveil the edge modes concentrated along the boundaries of the nanotriangle and the pseudoradial breathing modes (RBMs) concentrated inside the nanotriangle cavity. We present the indexing of all these modes based on one- and two-dimensional Fabry–Perot cavity models. In analogy to the relation between disk edge modes and film edge modes,<sup>7,8</sup> we prove experimentally that nanotriangle edge modes are similar to the Surface Plasmon modes of linear nanoantennas having the same length as the edge of the triangle. A two-dimensional Fabry–Perot analytical model allows us to label RBMs in nanotriangles with a set of two quantum numbers. The dispersion relation of the triangles RBMs follows that of quasistatic stationary short-range surface plasmons (SRSPs)<sup>12</sup> in thin films, as in the case of disk RBMs.<sup>7,8</sup>

## SAMPLE AND EXPERIMENT DETAILS

To ease the measurement of a wide range of modes, we take advantage of aluminum, which sustains plasmon resonances with a high spectral separation from infrared to UV (up to 6

Received: March 6, 2017

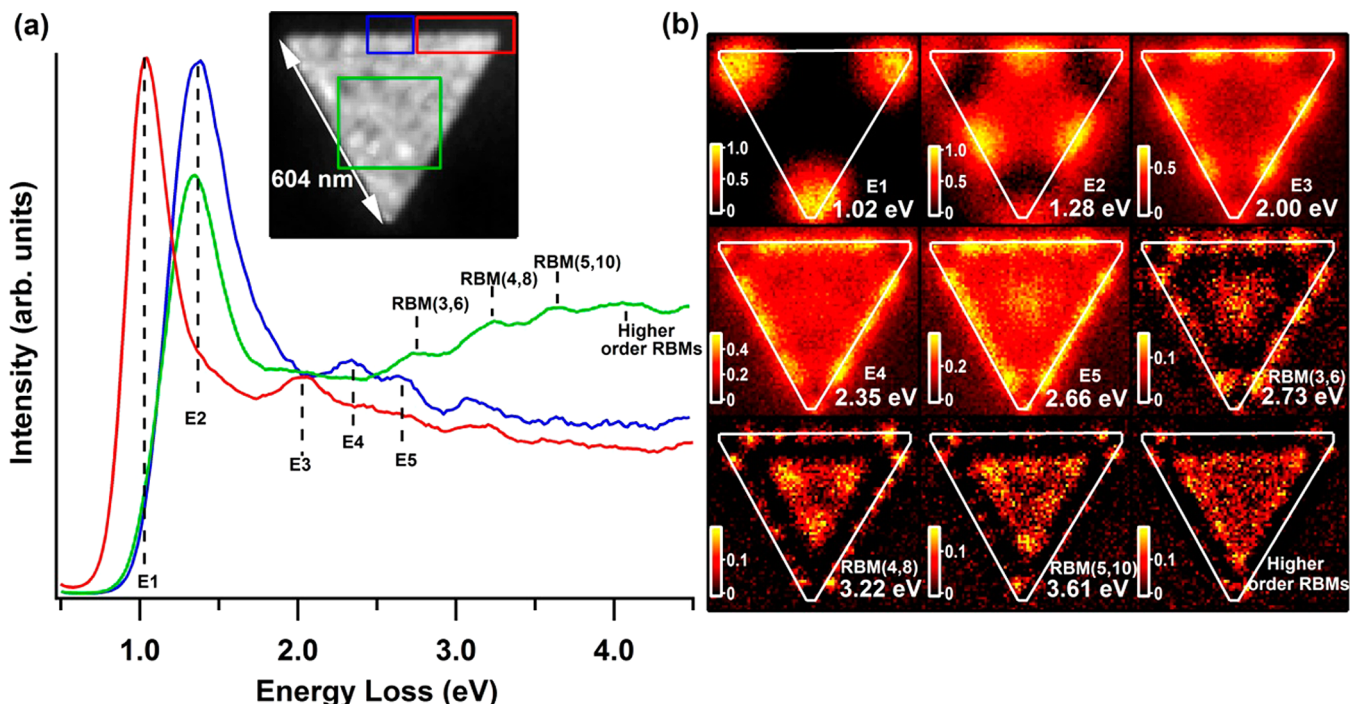


**Figure 1.** (a) Deconvoluted EEL spectra acquired at different locations (color boxes in the inset) on a single Al nanotriangle with 604 nm side length. The labels E and RBM stand for the edge and pseudoradial breathing modes observed in the nanotriangle. Inset: corresponding HAADF image. (b) EELS fitted intensity maps of the plasmon resonances sustained by the Al nanotriangle at the energy of the resonances evidenced in a.

eV) and allows us to distinguish properly the edge and the RBMs. Aluminum equilateral nanotriangles were fabricated by electron beam lithography and lift-off process on a STEM-EELS compatible substrate (30 nm thick  $\text{Si}_3\text{N}_4$  membrane). The triangle side length varies from 125 to 700 nm, while the thickness of all structures is 40 nm. EELS measurements were carried out using a NION USTEM 200 scanning transmission electron microscope (STEM) fitted with a cold field emission gun. Throughout this study, we used a 100 kV acceleration voltage. Typically, the electron probe current was 20 pA and the electron probe diameter was of the order of 1 Å. Data were acquired in the so-called spectral image mode (SI), in which an EEL spectrum is acquired at each pixel of a scan. At the end of the scan, both a spectral image and a high-angle annular dark field (HAADF) image are generated, which can be compared pixel per pixel. Dwell times per pixel and SIs sizes were typically 8–10 ms and  $100 \times 100$  pixels, respectively. In order to keep the same aspect ratios and number of pixels for each SI, we adapted the spatial sampling to the varying sizes of the structures. Although the spectral resolution of our EELS spectrometer is 0.4 eV, the systematic use of Richardson–Lucy Deconvolution<sup>19</sup> (with typically 50 iterations) yields a ~0.15 eV spectral resolution. Finally, an automatic fitting procedure with several Gaussian functions (using the open source software hyperspy 0.8.1) was used to generate the intensity maps.<sup>20</sup>

## RESULTS AND DISCUSSION

Figure 1a presents typical deconvoluted EEL spectra measured at different points on the same aluminum nanotriangle with a 604 nm side length. The upper inset contains the HAADF image with three boxes in which the EEL spectra were measured. The spectra are therefore the sum of individual spectra (one per pixel) contained in the boxes. Figure 1a reveals

distinct and well-defined energy loss peaks with maxima between 1 and 4 eV. These features correspond to the multipolar plasmonic resonances sustained by the Al nanotriangles. The resonances obtained at the edges of the triangle (curves blue and red in Figure 1a) are in good agreement with even and odd multipolar plasmonic resonances reported previously in Al nanoantennas.<sup>21</sup> The spectrum measured on the central part of the nanotriangle (green box) presents a background that comes from the tail of a broad peak centered at 7 eV, which corresponds to the plasmon of an aluminum thin film (see Figure S1 in the Supporting Information).

The spectra were fitted with Gaussian functions. While fitting the spectrum coming from the center of the triangle (green box), we used a linear background in order to remove the contribution from the low energy tail of the high intensity surface plasmon in aluminum thin films (see Supporting Information, Figure 1). In Figure 1b, the spatial symmetry of the modes is further analyzed by mapping the intensity of the Gaussian functions used in the fits. This has been reproduced on all nanotriangles of different sizes investigated in this study. These intensity maps are directly linked to the projection onto the electron beam trajectory of the electromagnetic local density of states (EMLDOS).<sup>22</sup> Gaussian functions were used in the curve fittings instead of the Lorentzian functions due to the fact that the improvement of the spectral resolution by the deconvolution process is not sufficient to converge toward the well-known Lorentzian line shape of surface plasmon resonances.

A closer look at the intensity distribution maps evidences two kinds of modes: edge modes located at the edge of the nanotriangle and the pseudo-RBM modes located inside the triangular cavity and confined by the triangle boundaries.

Before discussing the behavior of edge modes and RBMs as a function of the size of the triangle, we need to introduce a

robust indexing scheme. For the edge modes, we adopt an indexing based on a one-dimensional Fabry–Perot model. This approach was already used to describe nanoantenna modes<sup>23,24</sup> and film edge modes.<sup>7</sup> To index the RBMs, we extend to the case of plasmonic cavities a classification that was previously proposed for photonic cavities.<sup>25,26</sup> Intensity maps of edge modes can be interpreted as arising from a constructive interference in a one-dimensional Fabry–Perot cavity. The constructive interference is obtained whenever half the wavelength of the surface plasmon (SP) wave fits into the edge length. This condition yields the following relation between the SP wavenumbers ( $k_n$ ) for the edge modes:<sup>23</sup>

$$k_n L = n\pi - \phi \quad (1)$$

where  $n$  is an integer,  $L$  is the length of the cavity, and  $\phi$  is the phase shift upon reflection at the boundaries of the cavity. In the following, the different edge mode orders are labeled  $E_n$  ( $E_1, E_2, E_3, \dots$ ). It is worth noting that these modes only depend on  $L$ , which will be proven later. In that sense, they behave just like multipolar modes in linear nanoantennas and do not depend on the general symmetry of the nanoparticle. We will prove experimentally later that the dispersion relation of edge modes in nanotriangles is identical to the dispersion relation of nanoantenna modes, provided  $L$  stands for the length of the nanoantenna or the edge length of the triangle. This validates the use of eq 1 in nanotriangle edge modes. In contrast, the pseudo-RBMs exhibit a 3-fold symmetry pattern within the nanotriangle due to its specific geometry and boundary conditions. To describe the pseudo-RBMs, we use a triangular two-dimensional Fabry–Perot cavity model. We adopt the approach initiated by Chang et al.<sup>25</sup> and Wysin<sup>26</sup> to describe micro-sized dielectric cavities with applications as microlasers and resonators. In Wysin's paper, the electromagnetic modes of equilateral triangle resonators are investigated using a set of six plane waves in the triangle matched to each other by Fresnel factors and producing evanescent waves outside the triangle. In the present case, we consider the sequential reflections of a surface electromagnetic wave on the edges of a triangular cavity. However, we need to reinterpret the analytical model derived by Wysin to the case of plasmon waves, which are in this case quasi-static stationary short-range surface plasmons (SRSPs)<sup>12</sup> and not necessarily propagating modes (more details about the analytical model are given in *Supporting Information, section 2*). Contrary to the case of semiconductor microstructures embedded in air, the confinement is therefore not caused by total internal reflection but it is due to the confinement of the SRSPs at the surfaces of the aluminum nanotriangles.

The electric field inside the triangular cavity can be written as the sum of the contributions from the six different plasmon waves (SRSPs):

$$E_{\text{SRSP}} = \sum_{i=1}^6 E_{\text{SRSP},i} e^{ik_i \cdot r} \quad (2)$$

The analytical model<sup>26</sup> provides the wavenumbers of the SRSP eigenmodes formed in a triangular Fabry–Perot cavity:

$$k_{l,m} L = \frac{2\pi}{3} \left[ (m-l)^2 + 3 \left( \frac{m+l}{3} - \frac{2\varphi}{\pi} \right)^2 \right]^{1/2} \quad (3)$$

where  $l$  and  $m$  are integers,  $L$  is the side length of the triangle, and  $\varphi$  is the phase shift upon reflection at the edges of the triangle (the phase shift is assumed independent of the

incidence angle on the edges of the triangle). In the following, the pseudo-RBMs are labeled  $\text{RBM}_{(l,m)}$ . The symmetry of the first, second and third RBM of the intensity maps (Figure 1b) can be obtained in the analytical model with the following integers  $\text{RBM}_{(3,6)}$ ,  $\text{RBM}_{(4,8)}$ , and  $\text{RBM}_{(5,10)}$ , respectively, and a phase shift of  $0.45\pi$ . This was obtained by best matching the spatial distribution of electric field coming from eq 2 with experimental intensity maps while changing the phase shift. Figure 2 shows the comparison between the experimental EELS

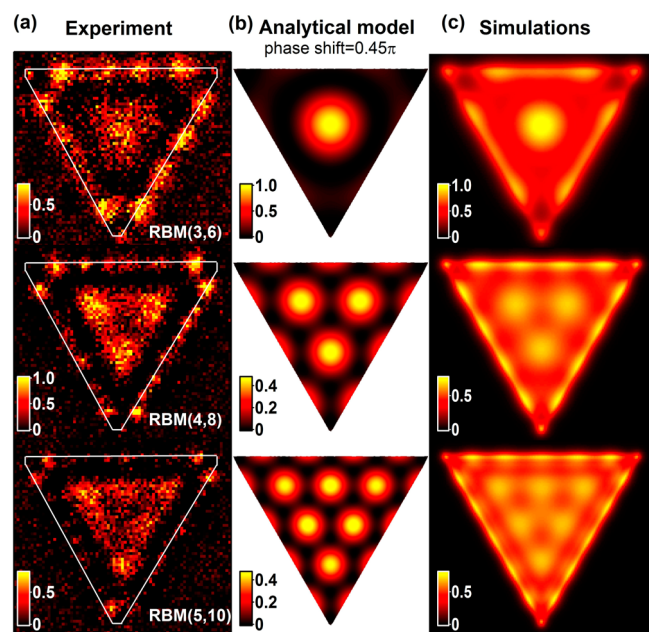


**Figure 2.** (a) Experimental maps of the RBMs of an aluminum nanotriangle of 604 nm side length. (b) Analytical model maps obtained with a phase shift of  $0.45\pi$  showing the good agreement with experimental maps. (c) EELS-GDM simulations maps computed at the energy of the RBMs.

intensity maps and the intensity maps obtained with the analytical model. It was observed that the distances between central lobes in  $\text{RBM}_{(4,8)}$  and  $\text{RBM}_{(5,10)}$  in the analytical model match very well with the experimental maps using a phase shift of  $0.45\pi$ . The fact that the phase shift is different from zero reveals that the reflection of the SRSP could be affected by charge accumulation at the boundaries or by field extension into the vacuum.<sup>23</sup> It is important to remark that between the RBMs observed experimentally, the analytical model predicts RBMs that we do not observe experimentally. This result is related to the fact that the RBMs observed experimentally yield the highest values of the EMLDOS (*Supporting Information, section 2*). The experimental EELS and analytical maps (Figure 2a and b, respectively) were also compared with extensive electrodynamic simulations using the EELS-Green Dyadic Method (EELS-GDM)<sup>27</sup> (Figure 2c). This technique relies on the computation of a so-called generalized field propagator from which several aspects of the interaction of the beam of fast electrons can be accurately described (more details about the GDM simulations are given in *Supporting Information, section 3*). As it can be observed, the experimental, GDM simulated and analytical model maps match very well for the RBMs inside the triangle. However, on the edge of the triangle we do not observe the same number of lobes. This is expected for the 2D analytical model which does not take into account the edge

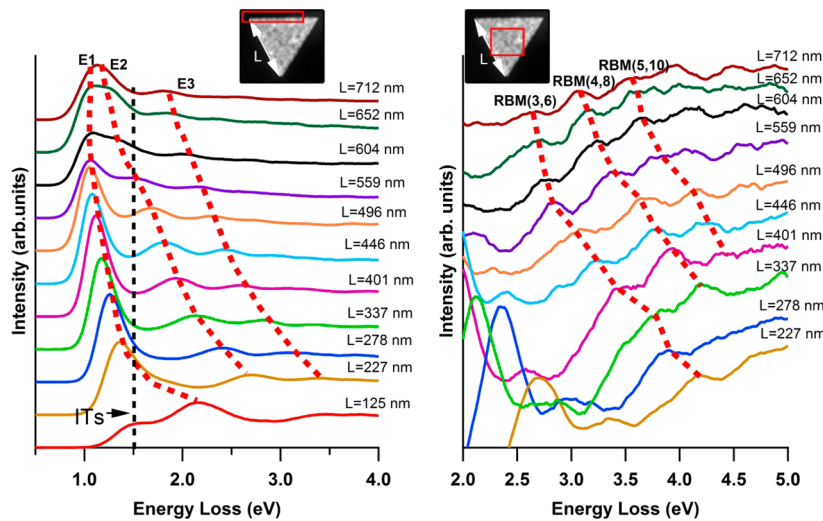


**Figure 3.** Dispersion of the plasmonic edge modes and pseudo-RBMs with varying triangle side lengths. (a) EEL spectra measured on the edge of triangles of different edge lengths. The dashed red lines follow the spectral position of different edge modes and the black dashed line corresponds to the position of interband transitions in aluminum. (b) EEL spectra taken on the center of triangles for different length sizes. The dashed red lines follow the spectral position of different RBMs.

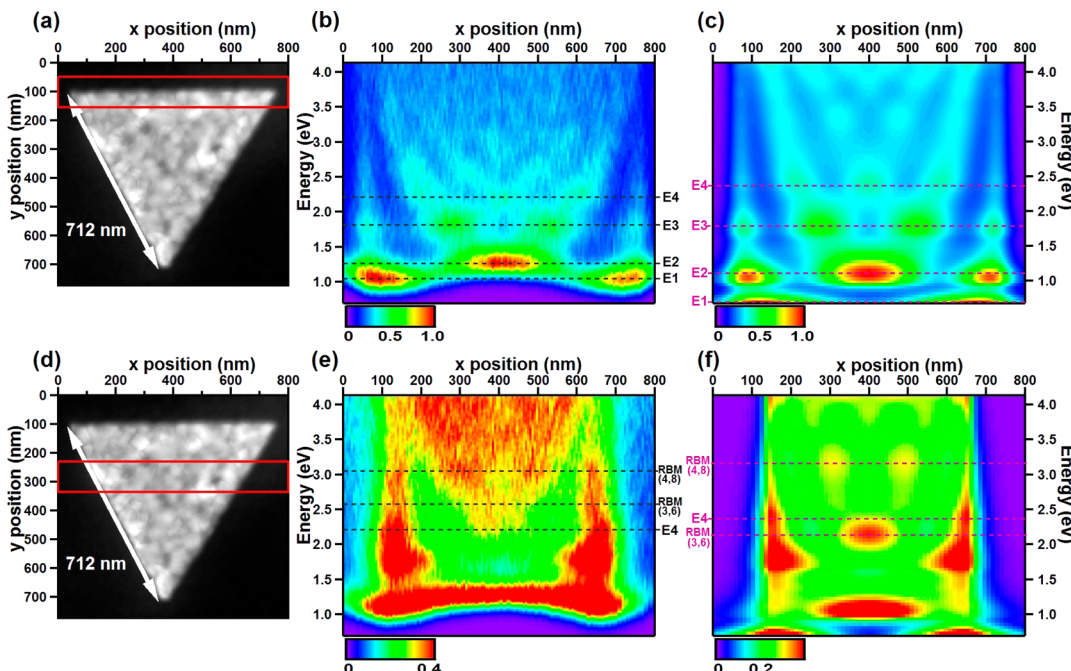


**Figure 4.** (a) HAADF images of an Al nanotriangle of around 700 nm side length. The red box indicates the region studied to obtain the dispersion of edge modes along  $x$  axis. (b) Energy dispersion along the  $x$  axis marked by the red box in a. (c) EELS-GDM dispersion simulation of a triangle of 700 nm side length along the edge of the triangle. (d) Same HAADF image as in a. The red box is placed close to the center of the triangle in order to obtain the dispersion of RBMs. (e) Energy dispersion along the  $x$  axis marked by the red box in d. Intensity has been saturated in order for the faint features at high energy to be visible. (f) EELS-GDM dispersion simulation of a triangle of 700 nm side length along a horizontal line close to the center of the triangle. The energy ranking change for RBM<sub>(3,6)</sub> and E<sub>4</sub> between experiment and simulation is made explicit.

modes at all, as they are separately simulated as 1D cavity modes, as presented before. In the experimental and GDM simulated maps the number of visible lobes on the edges is different, which is likely due to an energy inversion of some modes in the simulations that we will discuss later in Figure 4. In ref 28, a similar two-dimensional model has been used to describe modes in large triangular cavities. In this case, the modes were completely different (surface plasmon polaritons at the surface of an infinite silver plane) and confined by silver reflector blocks separated by micrometric distances. The phase

shift upon reflection was  $\sim\pi$ , revealing radically different boundary conditions (Dirichlet condition).

To obtain the dispersion of the edge modes and RBMs, we studied Al nanotriangles with side lengths varying from 125 to 700 nm. The EEL spectra measured at the triangles' edges and triangles' centers are shown in Figure 3a and b, respectively. For both kinds of modes, a monotonous shift of the plasmon modes peaks toward higher energies when the triangle size decreases is evidenced. The different edge modes and RBMs are labeled and their evolution (or energy shift) is highlighted

by the red dashed curves, unveiling their dispersion behavior. These results show the tunable properties of the edge modes in the visible-infrared region and the RBMs in the UV region by varying triangle size. Note that an additional peak around 1.5 eV is visible in the smaller triangle of Figure 3a. This feature is associated with interband transitions (ITs) in aluminum. It has been observed that ITs in aluminum can strongly couple with Surface Plasmons, resulting in convoluted features.<sup>21,29</sup> We observe qualitatively in Figure 3a a slight increase of the line width of  $E_1$  when it is centered close to the ITs.

In order to support spectral-space observations of both edge modes and pseudo-RBMs, we performed EELS-GDM simulations taking into account the  $\text{Si}_3\text{N}_4$  substrate (Supporting Information include a movie of the EELS simulated maps evolution with energy). Figure 4 shows the experimental and simulated energy dispersion along the horizontal axis placed at two vertical positions on an Al nanotriangle of 700 nm side length. The dispersion relations were obtained in the following way: spectra across the height of the red rectangles in Figure 4a,d were integrated, and their intensity as a function of the energy and position along the horizontal axis was plotted in Figure 4b,e. Figure 4c,f presents the corresponding simulated energy dispersion. As it can be observed by comparing Figure 4b and c, the edge modes are very well reproduced by the simulations showing a pattern very close to that of the experiments. However, the simulated energy spacing is larger than the experimental one. This relatively larger energy spacing is expected at energies smaller than 1 eV due to the limitation of the deconvolution process to separate peaks. This is reflected in the overlap of  $E_1$  and  $E_2$  for increased triangle side lengths (Figure 3a). The experimental RBMs dispersion is also very well reproduced by simulations (Figure 4f) along a horizontal line close to the center of the triangle. However, again the energy spacing is higher in simulations than in experiments. Differences between the dielectric data taken into account in the simulations and the real ones partly explain this discrepancy. In particular, the refractive index of the  $\text{Si}_3\text{N}_4$  substrate may have been slightly underestimated in the UV-blue spectral range. Setting aside the difference in energy spacing, the only discrepancy in the simulations is an inversion in energy of the first RBM ( $\text{RBM}_{(3,6)}$ ) with the fourth edge mode ( $E_4$ ). However, this mismatch could be explained due to the native oxide shell of aluminum which is not taken into account in simulations. It could also be due to the shape of the triangle edge used in the computation.

To further understand the nature of edge modes and RBMs, we study the dispersion relation (energy vs wavenumber) for both kinds of modes. By using eqs 1 and 3, it is possible to get a robust and sound definition of the wavenumbers of the edge modes and the RBMs. Edge modes phase shifts are calculated by fitting the profiles of intensity maps with a simple model of an incident and a phase shifted reflected plasmon wave inside a linear Fabry–Perot cavity (Supporting Information, section 4). From eq 1, we then obtain the wavenumber. This approach ignores the antinode bunching effect<sup>21,23</sup> at the triangle corners (see Figure S5 in the SI). We have observed that the phase shift of the edge modes has a tendency to decrease with increasing the mode order from around  $0.45\pi$  to  $0.15\pi$  (see Figure S6 in the SI). This decrease in phase shift has also been reported in silver nanorods.<sup>23</sup> It means that higher order edge modes are more confined at the edge of the triangle. This behavior differs from the case of RBMs where the phase shift is constant independently of the mode order. RBMs and edge modes phase

shifts have equivalent values at low order. RBMs wavenumbers are calculated by eq 3 using the constant phase shift of  $0.45\pi$  and the integers  $\text{RBM}_{(3,6)}$ ,  $\text{RBM}_{(4,8)}$ , and  $\text{RBM}_{(5,10)}$ .

Figure 5 shows the dispersion relation ( $E$  vs  $k$ ) for edge modes and RBMs in Al nanotriangles. These two kinds of

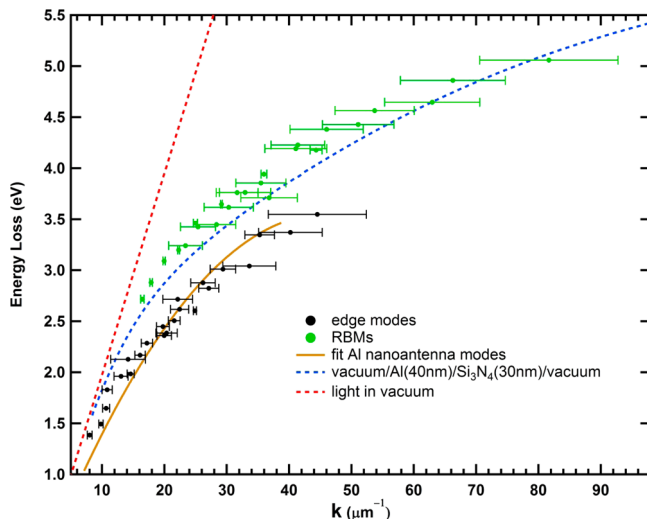


**Figure 5.** Dispersion relation of the edge modes and pseudo-RBMs of Al nanotriangles. The solid brown curve is obtained by fitting the experimental dispersion relation of Al nanoantenna modes. The dashed blue curve is the analytical dispersion relation of an Al thin film (40 nm thickness) on a  $\text{Si}_3\text{N}_4$  substrate (30 nm thickness) immersed in vacuum. We observe that Al edge nanotriangles modes and Al nanoantenna modes match very well. An analogous match is observed between RBMs and the analytical dispersion relation of an Al thin film.

modes present different dispersion relations, highlighting their different natures. To complement this study, we have measured Al nanoantenna dispersion relation with the same analysis used for edge modes in nanotriangles using eq 1. Al linear nanoantennas<sup>21</sup> have been prepared with the same method as for Al nanotriangles and characterized by EELS using the same experimental parameters (see ref 21). We did a third-order polynomial fit of the Al nanoantenna dispersion (see Figure S7 in the SI) and it was placed in Figure 5 as a guide for eye (solid brown curve). Both triangle edge modes dispersion and Al nanoantenna modes dispersion match very well. On the other hand, the RBMs can be compared with the analytical dispersion relation of an Al thin film (40 nm thickness) on a  $\text{Si}_3\text{N}_4$  substrate (30 nm thickness) immersed in vacuum (blue curve).<sup>30</sup> A similar agreement between the dispersion relation of RBMs and a thin film has been reported in the literature in silver nanodisks.<sup>7,8</sup> The difference in energy of the dispersion relation of RBMs and edge modes is due to the fact that RBMs come from the interference of Short Range Surface Plasmon and therefore they follow the dispersion relation of a thin film. However, edge modes are scaled to the case of nanoantenna modes.

## CONCLUSION

In summary, we used STEM-EELS to characterize plasmonic resonances supported by Al nanotriangles. Two kinds of modes have been observed, the edge modes and the pseudo-RBMs. Studying different triangles sizes (from 125 to 700 nm side length) we found tunable plasmon resonances from IR to UV range. Edge modes are more tunable in the IR-visible range and

the RBMs in the UV range. The symmetry of these modes and their energy dispersion have been theoretically verified by rigorous EELS-GDM simulations. One dimensional and two-dimensional Fabry–Perot analytical models allowed us to label the edge modes and RBMs and to study the phase shift upon reflection. The RBMs phase shift is found independent from the order mode, exhibiting a value of  $\sim 0.45\pi$ . Finally, the wavenumbers extracted from the linear and triangular resonator models were used to plot the dispersion relation ( $E$  vs  $k$ ) of edge modes and RBMs. The different behavior in the dispersion relation of both modes reveals their distinct nature. It has been proven experimentally (for the first time) that edge modes in Al nanotriangles can be related to Al nanoantenna modes. On the other hand, the RBMs have been related to the dispersion relation of a thin film. We not only described the symmetry of these modes but went into details in the phase shift upon reflection of the plasmon waves.

## ASSOCIATED CONTENT

### Supporting Information

The Supporting Information is available free of charge on the ACS Publications website at DOI: [10.1021/acspophotonics.7b00204](https://doi.org/10.1021/acspophotonics.7b00204).

Supporting movie (AVI).

(1) Breathing Modes Curve Fitting; (2) Analytical Model of Plasmonic Triangular Resonators; (3) EELS-GDM Simulations; (4) Analytical Model of Edge modes in Nanotriangles (PDF).

## AUTHOR INFORMATION

### Corresponding Author

\*E-mail: [mathieu.kociak@u-psud.fr](mailto:mathieu.kociak@u-psud.fr).

### ORCID

Jérôme Martin: [0000-0001-6761-5841](https://orcid.org/0000-0001-6761-5841)

Mathieu Kociak: [0000-0001-8858-0449](https://orcid.org/0000-0001-8858-0449)

### Notes

The authors declare no competing financial interest.

## ACKNOWLEDGMENTS

Experiments have been performed within the frame of the METSA Federation (FR3507). This work was supported by the computing facility center CALMIP of the University Paul Sabatier of Toulouse and ANR through Grant ANR-14-CE26-0013. Samples were fabricated at Nano'mat ([www.nanomat.eu](http://www.nanomat.eu)), which is supported by the Région Champagne-Ardenne, the Conseil Général de l'Aube, and FEDER funds from the European Community. D.G. is supported by the Région Champagne-Ardenne.

## REFERENCES

- Atwater, H.; Polman, A. Plasmonics for improved photovoltaic devices. *Nat. Mater.* **2010**, *9*, 205–213.
- Carles, R.; Bayle, M.; Benzo, P.; Benassayag, G.; Bonafos, C.; Cacciato, G.; Privitera, V. Plasmon-Resonant Raman Spectroscopy in Metallic Nanoparticles: Surface-Enhanced Scattering by Electronic Excitations. *Phys. Rev. B: Condens. Matter Mater. Phys.* **2015**, *92*, 174302.
- Lal, S.; Link, S.; Halas, N. Nano-Optics from Sensing to Waveguiding. *Nat. Photonics* **2007**, *1*, 641–648.
- Martin, J.; Proust, J.; Gérard, D.; Plain, J. Localized Surface Plasmon Resonances in the Ultraviolet from Large Scale Nanostructured Aluminum Films. *Opt. Mater. Express* **2013**, *3*, 954–959.
- Sanz, J. M.; Ortiz, D.; Alcaraz de la Osa, R.; Saiz, J. M.; González, F.; Brown, A. S.; Losurdo, M.; Everitt, H. O.; Moreno, F. UV Plasmonic Behavior of Various Metal Nanoparticles in the Near- and Far-Field Regimes: Geometry and Substrate Effects. *J. Phys. Chem. C* **2013**, *117*, 19606–19615.
- Huang, Y.; Chen, W. T.; Tsai, W.; Wu, P. C.; Wang, C.; Sun, G.; Tsai, D. P. Aluminum Plasmonic Multicolor Meta-Hologram. *Nano Lett.* **2015**, *15*, 3122–3127.
- Schmidt, F.-P.; Ditlbacher, H.; Hohenester, U.; Hohenau, A.; Hofer, F.; Krenn, J. R. Universal Dispersion of Surface Plasmons in Flat Nanostructures. *Nat. Commun.* **2014**, *5*, 3604.
- Schmidt, F.-P.; Ditlbacher, H.; Hohenester, U.; Hohenau, A.; Hofer, F.; Krenn, J. R. Dark Plasmonic Breathing Modes in Silver Nanodisks. *Nano Lett.* **2012**, *12*, 5780–5783.
- Gu, L.; Sigle, W.; Koch, C. T.; Ögüt, B.; Van Aken, P. A.; Talebi, N.; Vogelgesang, R.; Mu, J.; Wen, X.; Mao, J. Resonant Wedge-Plasmon Modes in Single-Crystalline Gold Nanoplatelets. *Phys. Rev. B: Condens. Matter Mater. Phys.* **2011**, *83*, 195433.
- Bellido, E. P.; Manjavacas, A.; Zhang, Y.; Cao, Y.; Nordlander, P.; Botton, G. A. Electron Energy-Loss Spectroscopy of Multipolar Edge and Cavity Modes in Silver Nanosquares. *ACS Photonics* **2016**, *3*, 428–433.
- Nelayah, J.; Kociak, M.; Stephan, O.; García De Abajo, J.; Tence, M.; Henrard, L.; Taverna, D.; Pastoriza-Santos, I.; Liz-Marzan, L. M.; Colliex, C. Mapping Surface Plasmons on a Single Metallic Nanoparticle. *Nat. Phys.* **2007**, *3*, 348–353.
- Nelayah, J.; Kociak, M.; Stephan, O.; Gequet, N.; Henrard, L.; García De Abajo, J.; Pastoriza-Santos, I.; Liz-Marzan, L. M.; Colliex, C. Two-Dimensional Quasistatic Stationary Short Range Surface Plasmons in Flat Nanoprisms. *Nano Lett.* **2010**, *10*, 902–907.
- Keast, V. J.; Walhout, C. J.; Pedersen, T.; Shahcheragh, N.; Cortie, M. B.; Mitchell, D. R. G. Higher Order Plasmonic Modes Excited in Ag Triangular Nanoplates by an Electron Beam. *Plasmonics* **2016**, *11*, 1081.
- Hao, E.; Schatz, G. C. Electromagnetic Fields around Silver Nanoparticles and Dimers. *J. Chem. Phys.* **2004**, *120*, 357–366.
- Kumar, A.; Fung, K. H.; Mabon, J. C.; Chow, E.; Fang, N. X. Excitation and Imaging of Resonant Optical Modes of Au Triangular Nanoantennas Using Cathodoluminescence Spectroscopy. *J. Vac. Sci. Technol., B: Nanotechnol. Microelectron.: Mater., Process, Meas., Phenom.* **2010**, *28*, C6C21.
- Fung, K. H.; Kumar, A.; Fang, N. X. Electron-Photon Scattering Mediated by Localized Plasmons: A Quantitative Analysis by Eigen-Response Theory. *Phys. Rev. B: Condens. Matter Mater. Phys.* **2014**, *89*, 045408.
- Pabitra, D.; Tapas, K. C.; Pond, J. Probing Higher Order Surface Plasmon Modes on Individual Truncated Tetrahedral Gold Nanoparticle Using Cathodoluminescence Imaging and Spectroscopy Combined with FDTD Simulations. *J. Phys. Chem. C* **2012**, *116*, 15610–15619.
- Koh, A. L.; Fernández-Domínguez, A. I.; McComb, D. W.; Maier, S. A.; Yang, J. K. W. High-Resolution Mapping of Electron-Beam-Excited Plasmon Modes in Lithographically Defined Gold Nanostructures. *Nano Lett.* **2011**, *11*, 1323–1330.
- Gloter, A.; Douiri, A.; Tencé, M.; Colliex, C. Improving Energy Resolution of EELS Spectra: an Alternative to the Monochromator Solution. *Ultramicroscopy* **2003**, *96*, 385–400.
- De la Peña, F.; Burdet, P.; Ostasevicius, T.; Sarahan, M.; Nord, M.; Fauske, V. T.; Taillon, J.; Eljarrat, A.; Mazzucco, S.; Donval, G.; Zagonel, L. Z.; Walls, M.; Iyengar, I. *Hyperspy 0.8.1*, Hyperspy, August 2015. <http://doi.org/10.5281/zenodo.27735>.
- Martin, J.; Kociak, M.; Mahfoud, Z.; Proust, J.; Gerard, D.; Plain, J. High-Resolution Imaging and Spectroscopy of Multipolar Plasmonic Resonances in Aluminum Nanoantennas. *Nano Lett.* **2014**, *14*, 5517–5523.
- García De Abajo, J.; Kociak, M. Probing the Photonic Local Density of States with Electron Energy Loss Spectroscopy. *Phys. Rev. Lett.* **2008**, *100*, 106804.

- (23) Rossouw, D.; Couillard, M.; Vickery, J.; Kumacheva, E.; Botton, G. A. Multipolar Plasmonic Resonances in Silver Nanowire Antennas Imaged with a Subnanometer Electron Probe. *Nano Lett.* **2011**, *11*, 1499–1504.
- (24) Barnard, E. S.; White, J. S.; Chandran, A.; Brongersma, M. L. Spectral Properties of Plasmonic Resonator Antennas. *Opt. Express* **2008**, *16*, 16529–16537.
- (25) Chang, H. C.; Kioseoglou, G.; Lee, E. H.; Haetty, J.; Na, M. H.; Xuan, Y.; Luo, H.; Petrou, A.; Cartwright, A. N. Lasing Modes in Equilateral-Triangular Laser Cavities. *Phys. Rev. A: At., Mol., Opt. Phys.* **2000**, *62*, 013816.
- (26) Wysin, G. M. Electromagnetic Modes in Dielectric Equilateral Triangle Resonators. *J. Opt. Soc. Am. B* **2006**, *23*, 1586.
- (27) Arbouet, A.; Mlayah, A.; Girard, C.; Des Francs, G. C. Electron Energy Losses and Cathodoluminescence from Complex Plasmonic Nanostructures: Spectra, Maps and Radiation Patterns from a Generalized Field Propagator. *New J. Phys.* **2014**, *16*, 113012.
- (28) Zhu, X.; Zhang, Y.; Zhang, J.; Xu, J.; Ma, Y.; Li, Z.; Yu, D. Ultrafine and Smooth Full Metal Nanostructures for Plasmonics. *Adv. Mater.* **2010**, *22*, 4345–4349.
- (29) Langhammer, C.; Schwind, M.; Kasemo, B.; Zoric, I. Localized Surface Plasmon Resonances in Aluminum Nanodisks. *Nano Lett.* **2008**, *8*, 1461–1471.
- (30) Kim, K. Y. *Plasmonics - Principles and Applications*; InTech, 2012.